Tellus SERIES B CHEMICAL AND PHYSICAL METEOROLOGY
PUBLISHED BY THE INTERNATIONAL METEOROLOGICAL INSTITUTE IN STOCKHOLM

# Meteorological controls on the diurnal variability of carbon monoxide mixing ratio at a mountaintop monitoring site in the Appalachian Mountains

*By* TEMPLE R. LEE[1]*, STEPHAN F. J. DE WEKKER[1], SANDIP PAL[1], ARLYN E. ANDREWS[2] and JONATHAN KOFLER[2], [1]*Department of Environmental Sciences, University of Virginia, Charlottesville, VA, USA;* [2]*NOAA Earth System Research Laboratory, Boulder, CO, USA*

(Manuscript received 15 September 2014; in final form 13 April 2015)

ABSTRACT

The variability of trace gases such as carbon monoxide (CO) at surface monitoring stations is affected by meteorological forcings that are particularly complicated over mountainous terrain. A detailed understanding of the impact of meteorological forcings on trace gas variability is challenging, but is vital to distinguish trace gas measurements affected by local pollutant sources from measurements representative of background mixing ratios. In the present study, we investigate the meteorological and CO characteristics at Pinnacles (38.61 N, 78.35 W, 1017 m above mean sea level), a mountaintop monitoring site in northwestern Virginia, USA, in the Appalachian Mountains, from 2009 to 2012, and focus on understanding the dominant meteorological forcings affecting the CO variability on diurnal timescales. The annual mean diurnal CO cycle shows a minimum in the morning between 0700 and 0900 LST and a maximum in the late afternoon between 1600 and 2000 LST, with a mean (median) daily CO amplitude of $39.2 \pm 23.7$ ppb (33.2 ppb). CO amplitudes show large day-to-day variability. The largest CO amplitudes, in which CO mixing ratios can change $>100$ ppb in $<3$ h, occur in the presence of synoptic disturbances. Under fair weather conditions, local- to regional-scale transport processes are found to be more important drivers of the diurnal CO variability. On fair weather days with northwesterly winds, boundary layer dilution causes a daytime CO decrease, resembling the variability observed atop tall towers in flat terrain. Fair weather days with a wind shift from the northwest to the south are characterised by an afternoon CO increase and resemble the variability observed at mountaintops influenced by the vertical transport of polluted air from adjacent valleys.

*Keywords: mountaintop monitoring, carbon monoxide, air quality, planetary boundary layer, vertical mixing, horizontal wind shift*

## 1. Introduction

Observations of atmospheric trace gas mixing ratios are required for many applications, including air quality models and inverse carbon transport models. An understanding of the trace gas variability and the factors affecting this variability is important for these applications (e.g. Seinfeld and Pandis, 2006; De Wekker et al., 2009; Steyn et al., 2012). A few hundred metres above the surface in flat terrain, trace gas mixing ratios decrease in the well-mixed convective boundary layer during the daytime. At these heights, measurements are representative of spatial scales on the order of $10^6$ km$^2$ in the afternoon (Gloor et al., 2001), which has led to the establishment of a network of tall towers with heights up to 500 m above ground level (agl). Whereas much of the focus of the network is on monitoring carbon dioxide ($CO_2$) to help reduce uncertainties in regional- to continental-scale carbon budgets (e.g. Bakwin and Tans, 1995), carbon monoxide (CO) and a suite of other trace gases are sometimes measured as well. CO is important because of its use as a tracer of anthropogenic emissions and because it is the main sink for hydroxyl radicals (OH) on the global scale (e.g. Thompson, 1992; Henne et al., 2008).

Trace gas measurements are also increasingly being made at mountaintops around the world (e.g. Levin et al., 1995;

*Corresponding author.
email: temple@virginia.edu
Responsible Editor: Kaarle Hämeri, University of Helsinki, Finland.



Citation: Tellus B 2015, **67**, 25659, http://dx.doi.org/10.3402/tellusb.v67.25659

Henne et al., 2008; Thompson et al., 2009; Ramonet et al., 2010; Andrews et al., 2014). Between 2004 and 2008, trace gas measurements began at mountaintops in the continental US in the Cascade Mountains (Jaffe et al., 2005), Rocky Mountains (De Wekker et al., 2009) and Appalachian Mountains (Lee et al., 2012). Mountaintops are often used for the measurement of background, or free atmospheric (FA) trace gas mixing ratios because, at times, mountaintops are located above the regional planetary boundary layer (PBL). Within the PBL, CO mixing ratios are often higher than within the FA because of near-surface anthropogenic emissions, biomass burning (e.g. Crutzen and Andrea, 1990) and CO production, which occurs via methane oxidation and the oxidation of organic compounds emitted from vegetation (e.g. Zimmerman et al., 1978; Seinfeld and Pandis, 2006). CO emissions within the PBL can be transported to nearby mountaintops via multiple dynamical forcings on a variety of spatiotemporal scales. Daytime convective mixing, upslope flows (De Wekker et al., 2009), mountain venting (e.g. De Wekker et al., 2004; Henne et al., 2004, 2005) and wind shifts on the mesoscale (e.g. Schmidt et al., 1996) to synoptic-scale (e.g. Zellwegger et al., 2003) influence trace gas mixing ratios on timescales of up to a few hours and reduce the degree to which mountaintop trace gas measurements are representative of background values (e.g. Brooks et al., 2012). Many studies have found that these transport processes result in a daytime increase in CO mixing ratios at mountaintops (e.g. Forrer et al., 2000; Gao et al., 2005; Balzani Lööv et al., 2008; Henne et al., 2008; Obrist et al., 2008). Daytime increases are also reported for other trace gases (e.g. Necki et al., 2003; Weiss-Penzias et al., 2006) and aerosols (e.g. Baltensperger et al., 1997; Lugauer et al., 1998).

Although previous work has focused on the trace gas and aerosol variability observed at tall mountaintops and those with high topographic prominence (e.g. Thoning et al., 1989; Baltensperger et al., 1997; De Wekker et al., 2009), there has also been considerable work describing the trace gas variability at low mountaintops (e.g. Schmidt et al., 1996, 2003; Thompson et al., 2009; Ramonet et al., 2010; Pillai et al., 2011). Whereas tall mountaintops typically remain above the regional PBL away from local trace gas sources and sinks (e.g. Baltensperger et al., 1997), low mountaintops oftentimes lie at the transition between the regional PBL and overlying FA. Thus, the trace gas variability at these locations is very complex (e.g. Schmidt et al., 1996). For many applications, it is important to differentiate periods when these mountaintops sample clean, pristine air masses from periods when local emission sources and transported contributions are sampled. This knowledge can, for example, provide an estimate of the contribution of fossil fuel emissions to the in-situ $CO_2$ variability (e.g. Bakwin and Tans, 1995) and improve the estimate of regional- to continental-scale carbon sources and sinks from inverse carbon transport models (e.g. Peters et al., 2007; Gerbig et al., 2009; Schuh et al., 2010; Lac et al., 2013).

In the current study, we present CO and meteorological observations from a recently established mountaintop monitoring site in the Appalachian Mountains that we refer to as Pinnacles. The objectives of this paper are to (1) investigate the dominant meteorological drivers affecting the diurnal CO variability at Pinnacles, and (2) contrast the characteristics of the CO variability at Pinnacles with those at other mountaintop sites, as well as with tall tower sites located in flat terrain. Following a previous study focusing on $CO_2$ observations from Pinnacles (Lee et al., 2012) and studies at other mountaintop locations (e.g. Schmidt et al., 1996; Pillai et al., 2011; Brooks et al., 2012), we hypothesise that the largest CO changes occur (1) during air mass changes that accompany cold front passages and (2) during the daytime under fair weather conditions when convective mixing and upslope flows transport CO-rich PBL air to the mountaintop. To investigate these hypotheses, we use 4 yr (2009–2012) of CO mixing ratio and meteorological measurements from Pinnacles. Following a discussion of the on-site measurements in Section 2, we provide an overview of the monthly and diurnal cycles of the meteorological variables and CO mixing ratios in Sections 3.1 and 3.2. In Section 3.3, we compare the amplitudes of the mean diurnal CO cycles at Pinnacles with the amplitudes observed at other mountaintop CO monitoring sites around the world. In Sections 3.4 and 3.5, we differentiate between days with the largest and days with the smallest CO changes and investigate the dominant meteorological forcings on these days. We conclude the paper with a discussion of our results and possible implications in Section 4.

## 2. Data and methods

### 2.1. Site description

Pinnacles (38.61 N, 78.35 W) is located 1017 m above mean sea level (msl) in the Shenandoah National Park (SNP) along the crest of the Virginia Blue Ridge Mountains in eastern US (Fig. 1a). The nearest potential CO emissions source is Skyline Drive, a scenic tourist road oriented southwest-northeast along the crest of the Blue Ridge Mountains 120 m southeast of Pinnacles. Other nearby CO emission sources include the town of Luray, with a population of about 5000, located 15 km west of Pinnacles in the Page Valley. Washington, DC, the nearest metropolitan area, is located 120 km northeast of Pinnacles. In addition to anthropogenic emissions, other regional CO sources include CO emissions from biomass burning in upwind regions (e.g. Crutzen and Andrea, 1990).

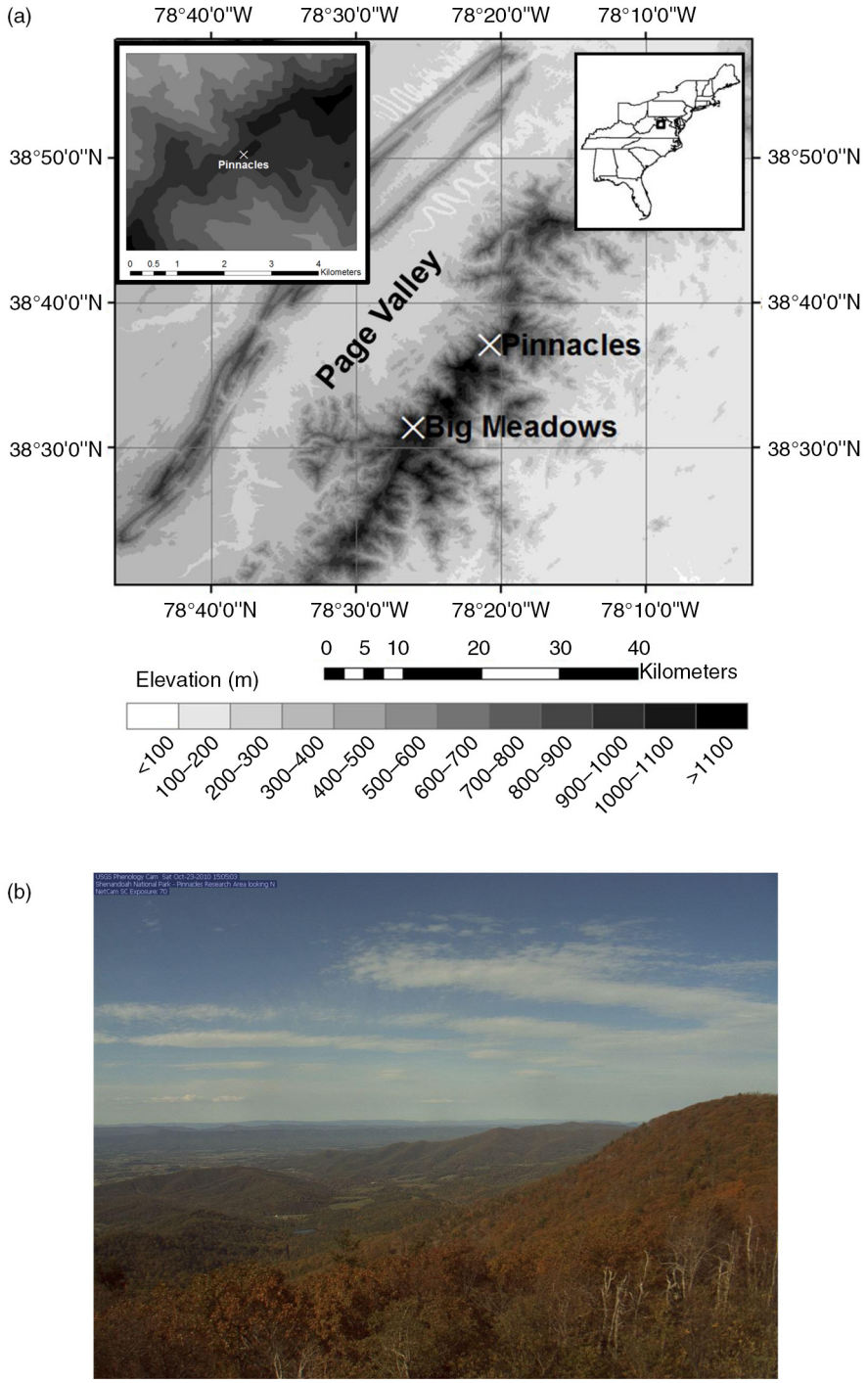


*Fig. 1.* Topographic map (a) indicating the location of Pinnacles (white X) relative to Big Meadows and the Page Valley. Shading shows elevation msl. The inset map at the top left shows the topography in a 5 km × 5 km box surrounding Pinnacles. The inset map at the top right indicates the study location, denoted by a black box, in the eastern US. Topography data are from the US Geological Survey and have a 10 m resolution. Panel (b) shows a web camera image taken at 1205 LST 23 Sept 2012 from the site showing the Page Valley northwest of Pinnacles.

### 2.2. *Trace gas measurements*

Pinnacles is part of the NOAA Global Greenhouse Gas Reference Network (http://www.esrl.noaa.gov/gmd/ccgg/). Measurements are made through collaboration with the NOAA Earth System Research Laboratory (ESRL). CO and $CO_2$ mixing ratios have been measured at 5, 10 and

17 m agl since August 2008 along a 17 m tower at the site. Both CO and $CO_2$ are sampled approximately every 10 min at each height, and half-hour means of these data are used in all analyses. In the present paper, we use data collected during the first four full years of measurements from 1 January 2009 to 31 December 2012. The CO and $CO_2$ data record over this period is 84% complete, as there are occasional gaps due to on-site power outages and miscellaneous system malfunctions.

CO and $CO_2$ are measured using a Thermo Electron Corporation 48C CO analyser and Li-COR 7000 closed path gas analyser, respectively. Instrumentation, calibration and measurement uncertainty are described in detail in Andrews et al. (2014). The measurements are fully automated, and NOAA-supplied field calibration standards are directly traceable to the World Meteorological Organization's mole fraction scales for CO and $CO_2$ maintained at the NOAA ESRL. The CO and $CO_2$ analysers both suffer from baseline drift, so the analyser baseline is measured every 30–40 min for CO and every 2 h for $CO_2$. The instrument calibration frequency has varied over the duration of the measurement period. Currently, the CO analyser is calibrated every 23 h using calibration standards of 100 ppb and 350 ppb. The $CO_2$ analyser is calibrated every 11 h using four standards: 350 ppm, 380 ppm, 410 ppm and 460 ppm. Additional target cylinders track measurement reproducibility at approximately 220 ppb (400 ppm) for CO ($CO_2$). Detailed uncertainty estimates and algorithms are provided in the data files available from NOAA ESRL (Andrews et al., 2014). Random and non-random (i.e. systematic) measurement uncertainties are reported separately during archival and post-processing. These uncertainties come from three sources: atmospheric trace gas variability, measurement uncertainty and scale uncertainty. The total uncertainty is the sum of these three uncertainties (Andrews et al., 2014). The atmospheric variability represents the standard deviation (SD) of the trace gas concentration over the 30-second period during which the trace gas of interest is sampled. Measurement uncertainty is a function of multiple systematic uncertainties, for example, differences in moisture content of the samples which can affect the measured trace gas concentration and extrapolation uncertainties that arise when trace gas samples are made that are outside the calibrated range of the monitoring system. The scale uncertainty arises from the uncertainties in the calibration standards themselves (Zhao and Tans, 2006). Total uncertainties are typically $<6$ ppb for CO and $<0.1$ ppm for $CO_2$ (Andrews et al., 2014).

In our analyses, we exclude data from periods when the analysers were performing poorly, which are rare but may occur, for example, during periods when the room temperature fluctuates significantly or when the trace gas observations are highly variable. Therefore, we compute a total uncertainty that is the quadrature sum of the non-random measurement uncertainty and the SD over the measurement period, which includes random analyser noise and real atmospheric variability. At Pinnacles, 82.7% (98.2%) of the CO measurements sampled at 17 m agl have a total uncertainty $<5$ ppb ($<10$ ppb), and 95.6% (99.9%) of the $CO_2$ measurements have an uncertainty $<0.1$ ppm ($<0.2$ ppm). We remove CO measurements whose total uncertainty exceeds 10 ppb.

### 2.3. *Meteorological measurements*

Meteorological measurements at Pinnacles began in July 2008 and include temperature, humidity, wind, radiation, pressure and rainfall (Table 1). Data from a CSAT sonic anemometer and a Li-COR 7500 water vapour and $CO_2$ gas analyser are used to compute 30 min mean sensible heat,

*Table 1.* Meteorological variable, sampling instrument, sampling height(s) and sampling technique for each meteorological variable measured at Pinnacles. Data from the CMP3 pyranometer are used to compute CI.

| Variable | Instrument | Sampling height(s) (m agl) | Sampling technique |
|---|---|---|---|
| Air temperature and humidity | Vaisala HMP45C | 2, 5, 10, 17 | 30 min means of 1 Hz samples |
| Barometric pressure | Vaisala CS105 pressure sensor | 14 | 30 min means of 1 Hz samples |
| $CO_2$ flux, latent heat flux | CSAT sonic anemometer, Li-COR 7500 water vapour and $CO_2$ gas analyser | 17 | 30 min means of 10 Hz samples |
| Incoming and outgoing shortwave and longwave radiation | Hukseflux 4-component net radiometer | 17 | 30 min means of 1 Hz samples |
| Incoming shortwave radiation | Kip and Zonen CMP3 pyranometer | 17 | 30 min means of 1 Hz samples |
| Rainfall | TR-525I tipping bucket rain gauge | 3 | 30 min total |
| Sensible heat flux | CSAT sonic anemometer | 17 | 30 min means of 10 Hz samples |
| Wind direction | MetOne 034B windset | 10, 17 | 30 min sample |
| Wind speed | MetOne 034B windset | 10, 17 | 30 min means of 1 Hz samples |

latent heat and $CO_2$ fluxes. To complement these measurements, a web camera was installed 17 m agl in October 2009 facing northwest into the Page Valley (Fig. 1b). Images are recorded every 15 min.

The meteorological data set is mostly complete ($>90\%$), but there are occasional gaps in the data due to data logger malfunctions and on-site power outages. Data quality assurance and quality control procedures include filtering the cup anemometer wind data by removing all wind measurements made when the wind speed is 0 m $s^{-1}$ for $>30$ min. Extended periods (sometimes $>12$ h) of 0 m $s^{-1}$ wind speeds are caused by rime ice on the instruments that occasionally occurs between October and April. Wind speeds of 0 m $s^{-1}$ for $>12$ h also occurred when the cup anemometer's potentiometer malfunctioned for several periods in summer 2009 and summer 2011. Because temperature and humidity are measured at multiple levels along the tower, we remove measurements that are unrealistically different from the others, and we remove flux measurements made during periods of precipitation.

Measurements of temperature, humidity, wind, insolation and precipitation from Big Meadows (38.52 N, 78.44 W, 1079 m msl), a mountaintop air quality monitoring site located 14 km south of Pinnacles (Fig. 1a), are used to fill in occasional gaps in the Pinnacles data record. Because frozen precipitation is not measured at Pinnacles but is a routine occurrence between October and April, we use precipitation data from Big Meadows (which has a heated rain gauge) to determine precipitation patterns.

### 2.4. Trajectory model

We run the Hybrid Single Particle Lagrangian Integrated Trajectory (HYSPLIT) model for a selection of cases discussed in Section 3.2 to understand source regions for periods of high CO mixing ratios. HYSPLIT is a kinematic backward trajectory model (Draxler and Hess, 2004) that we initialise using wind fields from the North American Model (NAM) (e.g. Janjic et al., 2010, 2011). The NAM has a horizontal grid spacing of 12 km and 60 vertical levels, 34 of which are below 5 km. Sensitivity tests using other meteorological models to provide the wind fields for HYSPLIT indicate that the source regions identified are unaffected by our choice of meteorological model. We initialise trajectories every hour for the time periods of interest and run trajectories backward for 72 h starting at 100 m agl. We choose 100 m agl because previous work at the site has shown that trajectory simulations with this starting height agreed best with observations from the site (Lee et al., 2012).

### 2.5. Reanalysis products

We use the North American Regional Reanalysis (NARR) to assist with the interpretation of our observations. NARR uses boundary conditions from the National Center for Environmental Prediction (NCEP) global reanalysis, NCEP Eta model, and surface and rawinsonde observations to generate meteorological fields over North America at a 32 km spatial resolution and 3 h temporal resolution. There are 29 vertical levels, 17 of which are below 5 km (Mesinger et al., 2006). NARR data are obtained from ftp.cdc.noaa.gov/NARR. Whereas higher resolution models such as the NAM are also available, NAM compares well with NARR over the region of interest (Lee, 2015) and thus we are confident in our choice to use NARR.

## 3. Results and discussion

### 3.1. Meteorological characteristics of the site

The region around Pinnacles is classified as humid subtropical in the Piedmont east of the Blue Ridge Mountains and is humid continental along and west of the Blue Ridge Mountains (e.g. Lee et al., 2012, 2014). At Pinnacles, mean afternoon temperatures 17 m agl range from $-2^{\circ}$C in January to 22°C in July (Fig. 2a). Water vapour mixing ratios 17 m agl are smallest (largest) in winter (summer), with mean values around 3 g $kg^{-1}$ (11.0 g $kg^{-1}$), and the mean daily amplitude is about seven times larger in summer than in winter. Rainfall is evenly distributed throughout the year, and total annual rainfall in 2009, 2010, 2011 and 2012 is 1396, 1467, 1493 and 1079 mm, respectively.

Mean afternoon sensible heat fluxes range from $<100$ W $m^{-2}$ in December to 250 W $m^{-2}$ in April (Fig. 2b). Latent heat fluxes begin increasing in April and are larger than the sensible heat fluxes from June to September, with the highest values near 300 W $m^{-2}$ in June. The latent heat fluxes agree with those reported by Lee et al. (2012) during the site's first year of measurements and with measurements reported at other mid-latitude continental locations located in similar climate regimes as Pinnacles (e.g. Greco and Baldocchi, 1996; Yi et al., 2001).

Mean wind speeds, averaged over 0000–2400 LST (UTC-5), are strongest in the winter (5.2 m $s^{-1}$) and weakest in the summer (2.8 m $s^{-1}$), and night-time winds are about 1 m $s^{-1}$ larger than daytime winds (Fig. 2c). Winds typically shift from the northwest at night to the south during the late afternoon, contributing to the bimodality in wind direction present in all seasons (Fig. 3).

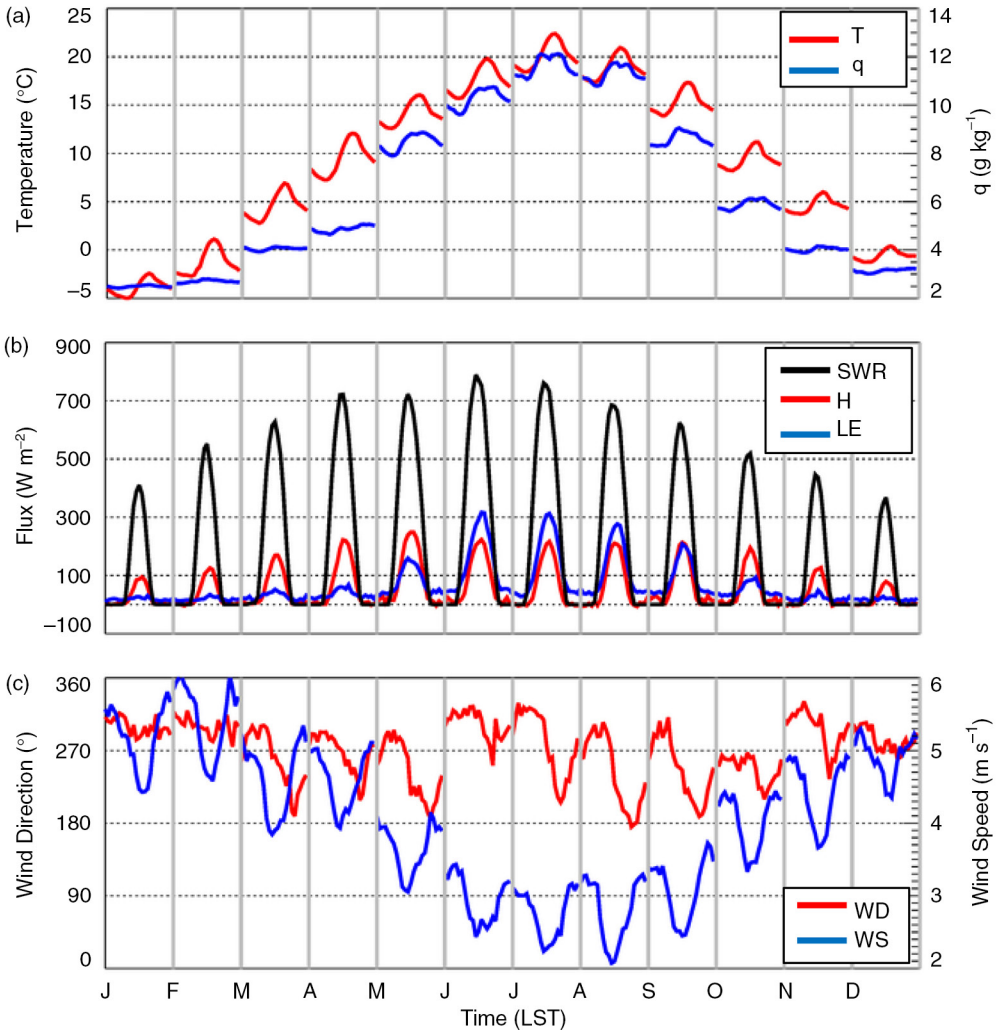


*Fig. 2.* Mean diurnal time series by month of temperature ($T$) (red line) and water vapour ($q$) (blue line) (a); shortwave radiation (SWR) (black line), sensible heat (H) (red line) and latent heat (LE) (blue line) (b); wind direction (WD) (red line) and wind speed (WS) (blue line) (c). Vertical grey lines distinguish different months. Means represent measurements from 1 January 2009 to 31 December 2012. All measurements are made at 17 m agl at Pinnacles. Sensible and latent heat fluxes $< -20$ W m$^{-2}$ are not included in the mean cycle. Because these are mean diurnal time series by month, the time series are discontinuous.

### 3.2. *Seasonal CO cycle*

Between 2009 and 2012, the mean CO mixing ratio at 17 m agl at Pinnacles was 144.3 ± 23.8 ppb. Annual mean (median) CO mixing ratios at 17 m agl in 2009, 2010, 2011 and 2012 were 139.2 ppb (137.7 ppb), 148.8 ppb (146.6 ppb), 145.1 ppb (144.0 ppb) and 144.7 ppb (144.8 ppb), respectively. Monthly mean CO at 17 m agl ranges from 160.3 ppb in March to 126.8 ppb in October (Table 2). CO mixing ratios are slightly higher near the surface. Mean CO mixing ratios measured at 5 m and 10 m agl are 146.6 ± 24.4 ppb and 145.4 ± 24.1 ppb, respectively, and exhibit the same diurnal and seasonal trends as the measurements at 17 m agl. In this paper, we focus on CO measurements made at 17 m agl.

The seasonal CO cycle is caused by the seasonality of OH, which peaks in the summer, and larger anthropogenic emissions during the winter (e.g. Novelli et al., 1998), and is consistent with other continental mid-latitude sites (e.g. Popa et al., 2010). The CO cycle is consistent from year-to-year (Fig. 4), but there are multiple times when the half-hour mean CO mixing ratio remains above one SD from the mean for >1 diurnal cycle. For example, over the period 7–11 August 2010, CO mixing ratios remained above 180 ppb, resulting in mean monthly CO mixing ratios that were higher in August 2010 than in other Augusts.

During these and other periods such as in late June 2012 (when CO mixing ratios remained >170 ppb for about 24 h), the elevated CO mixing ratios were mainly due to a

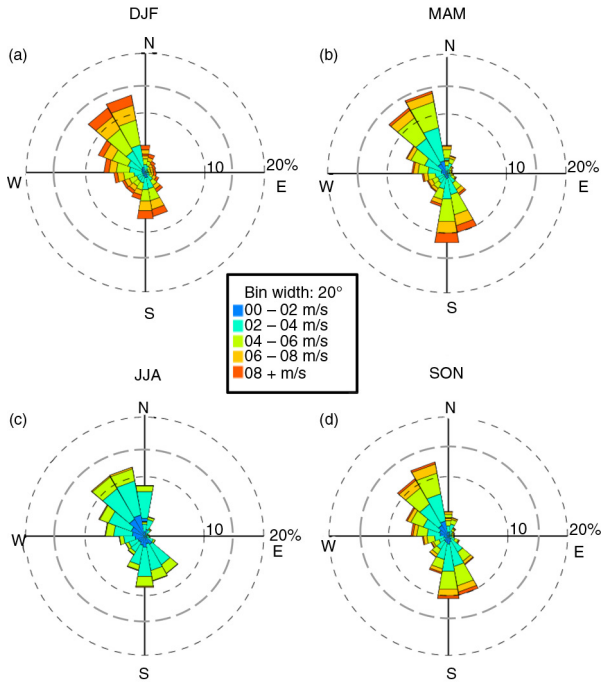


*Fig. 3.* Wind distribution at 17 m agl at Pinnacles in winter (DJF) (a), spring (MAM) (b), summer (JJA) (c) and fall (SON) (d) from 1 January 2009 to 31 December 2012. Data completion percentage is 83.2%, 86.8%, 58.5% and 79.2%, respectively.

combination of emissions from forest fires in the region and by the build-up of polluted air caused by weak synoptic forcing. We use output from the satellite-borne Moderate Resolution Imaging Spectroradiometer (MODIS), which provides information on the timing and locations of fires (e.g. Justice et al., 2002; Giglio et al., 2003). Output from MODIS indicates that forest fires were present a few tens to a few hundred kilometres upwind of Pinnacles during the periods of elevated CO mixing ratio. Furthermore, web camera images from Pinnacles showed hazy skies and reduced visibility over these periods, and synoptic analyses, as well as HYSPLIT backward trajectories, further corroborated weak near-surface anti-cyclonic flow.

In addition to cases when CO mixing ratios remain high for $>1$ diurnal cycle, there are multiple times when CO mixing ratios increase to values 2–3 times larger than the mean. These events happen on timescales $<3$ h; examples of these events are discussed in more detail in Section 3.4.

### 3.3. *Diurnal CO cycle*

On diurnal timescales, CO increases during the daytime, beginning around 0900 LST in the winter and 12 h earlier in the other seasons (Fig. 5). In all seasons, there is a maximum in the late afternoon-early evening that is followed by a night-time decrease. The mean diurnal CO cycle has the largest amplitude in the winter (7.1 ppb) and smallest amplitude in the summer (4.0 ppb). Mean daytime CO increases of this magnitude have been reported at other mountaintops (e.g. Forrer et al., 2000; Henne et al., 2008; Obrist et al., 2008) and are attributed to the vertical mixing and transport of valley PBL air to the mountaintop during the daytime. Nocturnal CO decreases at other mountaintops have been attributed to sinking motions that transport cleaner air from the FA to the mountaintop (e.g. Schmidt et al., 1996; Balzani Lööv et al., 2008).

In contrast with what we find at Pinnacles, previous studies reported larger mean daily CO amplitude in the summer than in winter because convective mixing is strongest during the summer (e.g. Atlas and Ridley, 1996; Forrer et al., 2000; Gao et al., 2005; Balzani Lööv et al., 2008; Henne et al., 2008). For example, at Mount Kenya (3678 m msl)

*Table 2.* Monthly mean and median CO; monthly mean and median afternoon (1200–1600 LST) CO; monthly mean and median night-time (0000–0400 LST) CO; and monthly maximum and minimum CO. All values are measured at 17 m agl at Pinnacles for the period 1 January 2009–31 December 2012.

| Month | Mean (median) CO (ppb) | Mean (median) afternoon CO (ppb) | Mean (median) night-time CO (ppb) | Maximum CO (ppb) | Minimum CO (ppb) |
|---|---|---|---|---|---|
| Jan | 156.7 (151.1) | 156.6 (150.7) | 155.6 (151.0) | 335.7 | 101.5 |
| Feb | 158.4 (156.5) | 158.5 (156.5) | 159.5 (157.2) | 250.4 | 98.3 |
| Mar | 160.3 (159.2) | 160.3 (159.0) | 161.0 (159.6) | 241.5 | 108.3 |
| Apr | 159.3 (156.4) | 157.5 (154.8) | 161.1 (157.7) | 448.9 | 94.9 |
| May | 146.3 (144.9) | 148.0 (145.1) | 146.3 (145.2) | 240.9 | 94.6 |
| June | 140.8 (136.9) | 140.9 (136.8) | 140.7 (137.6) | 224.8 | 82.8 |
| July | 135.9 (131.5) | 138.1 (133.6) | 134.6 (131.6) | 229.3 | 80.8 |
| Aug | 140.8 (137.9) | 141.2 (137.1) | 140.1 (138.6) | 289.5 | 76.6 |
| Sept | 131.8 (130.4) | 132.4 (129.6) | 132.0 (131.2) | 274.8 | 68.1 |
| Oct | 126.8 (124.7) | 127.0 (125.5) | 125.9 (124.4) | 254.5 | 80.4 |
| Nov | 138.4 (134.9) | 139.7 (136.9) | 137.9 (134.4) | 251.7 | 65.7 |
| Dec | 141.4 (139.4) | 142.7 (139.8) | 140.6 (138.5) | 289 | 96.4 |

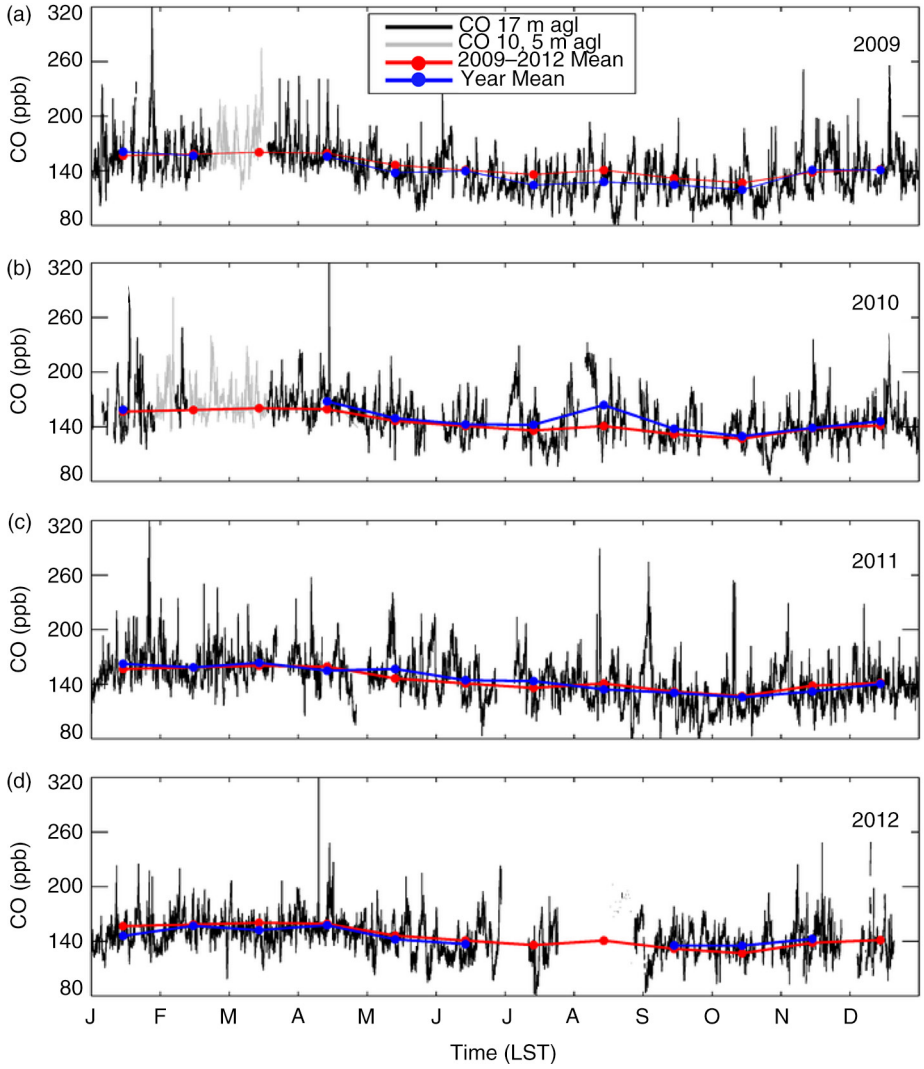


*Fig. 4.* Half-hour mean CO at 17 m agl at Pinnacles in 2009 (a), 2010 (b), 2011 (c) and 2012 (d) (black line). Data gaps have been filled in using data from 5 m and 10 m agl (grey line) when available. Superimposed red and blue lines represent monthly means for all years and the individual years, respectively, for months with >50% data completion. Data completion at 17 m agl for 2009, 2010, 2011 and 2012 is 89.2%, 74.7%, 93.1% and 78.3%, respectively. Measurements with an uncertainty >10 ppb are not shown.

in Africa, the amplitude of the mean diurnal CO cycle in the late summer (i.e. the dry season) is nearly double the amplitude of the mean diurnal cycle in the late winter (i.e. the wet season) (Henne et al., 2008). Larger diurnal CO amplitudes in the warm season have also been reported at tall mountaintops such as Mauna Loa (3397 m msl) in Hawaii (Atlas and Ridley, 1996), Jungfraujoch (3580 m msl) in the European Alps (Balzani Lööv et al., 2008).

To put our findings from Pinnacles into the context of findings from other mountaintops, we determine the relationship between the amplitude of mean diurnal CO cycle and the mountaintop's elevation above mean sea level using studies from seven other global mountaintop monitoring sites which report the mean diurnal CO amplitude as a function of season. We find a positive relationship between elevation and the mean diurnal CO amplitude (Table 3), indicating that taller mountaintops have higher CO amplitudes. The taller mountaintops are more strongly and/or more frequently influenced by FA air, which is cleaner than air in the adjacent valley PBL, particularly at night. Thus, on days when valley PBL air affects the mountaintop, which typically occurs during the daytime in the summer (e.g. Baltensperger et al., 1997; Lugauer et al., 1998), there is a larger change in the CO mixing ratio than there is when the mountaintop is unaffected by valley PBL air, which is typically during the winter.

However, there are many other factors besides elevation that affect the observed trace gas variability, including

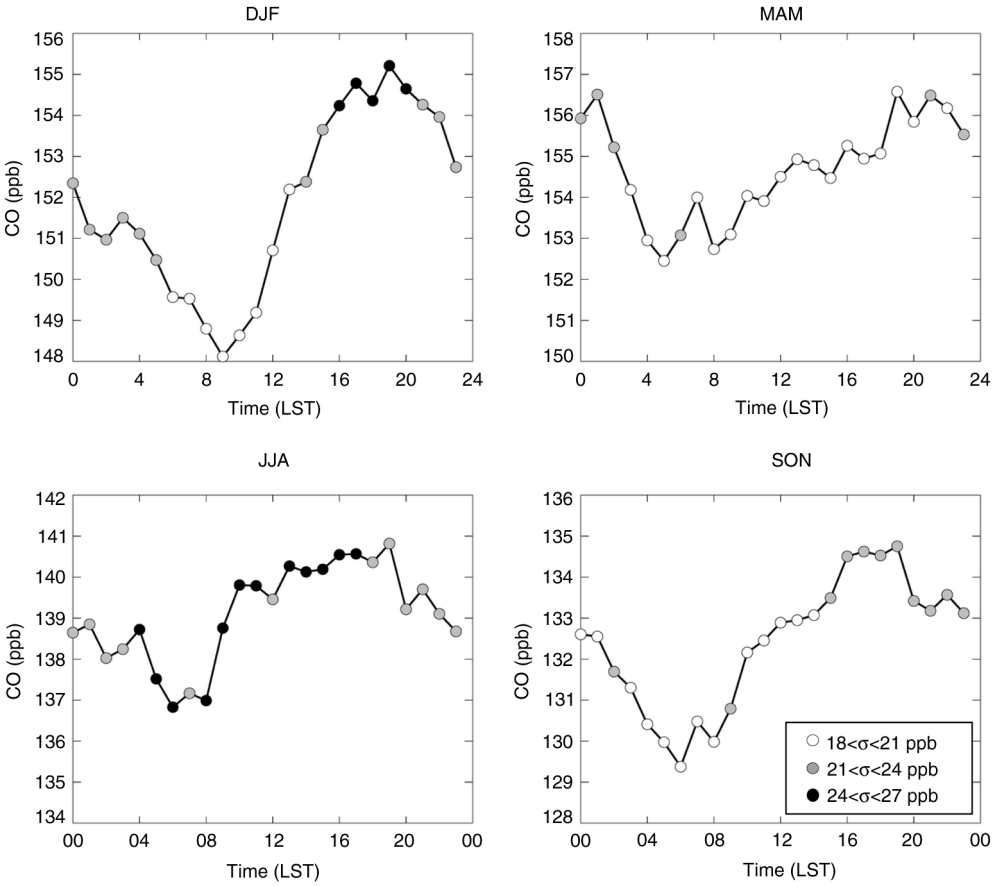


*Fig. 5.* Mean diurnal CO cycle at 17 m agl at Pinnacles from 1 January 2009 to 31 December 2012 in winter (DJF) (a), spring (MAM) (b), summer (JJA) (c) and fall (SON) (d). White, grey and black circles indicate standard deviations 18–21, 21–24 and 24–27 ppb, respectively. Data completion for winter, spring, summer, and fall is 80.7%, 84.7%, 78.4% and 91.9%, respectively. Note different values but the same range for each y-axis.

mountaintop shape (e.g. Igarashi et al., 2006), meteorological variability (e.g. Cooper and Moody, 2000; Lee et al., 2012; Pandey Deolal et al., 2014), PBL heights (Lee, 2015), and proximity to local emissions sources (e.g. Gao et al., 2005). For example, a mountaintop such as Mount Tai (1534 m msl) in China's Shandong province, despite its relatively low elevation, has a large mean diurnal CO cycle in the summer with a CO amplitude $>100$ ppb due to the site's proximity downwind of anthropogenic CO emissions (Gao et al., 2005). The effect of PBL heights is investigated in detail by Lee (2015), where he found increasing CO amplitudes at Pinnacles with decreasing boundary layer heights. The importance of meteorological variability to the diurnal CO behaviour is further investigated in the next section.

### 3.4. Daily CO amplitude variability

During the 4-yr period of interest, the CO amplitude, which we define as the difference between the daily maximum and daily minimum half-hour CO mixing ratio, ranged from 10.4 ppb to 293.7 ppb, and the mean (median) amplitude was $39.2 \pm 23.7$ ppb (33.2 ppb) (Fig. 6). Daily CO amplitudes are typically largest in winter ($44.4 \pm 26.2$ ppb) and smallest in summer ($36.7 \pm 18.4$ ppb) but show much variability around the mean. Daily amplitudes above the 90th percentile (i.e. $>67$ ppb), and therefore also the largest mean daily CO amplitudes, occur most often during the winter. Note that the daily CO amplitudes are much larger than the amplitude of the mean daily CO cycles because averaging removes some of the day-to-day CO variability.

We compare the days with the largest ($>90$th percentile) and the smallest CO amplitudes ($<10$th percentile) to determine the dominant meteorological forcings affecting CO variability during these types of days. Because of seasonal differences in CO mixing ratio and daily CO amplitude, we differentiate among seasons. Within any season, days with the smallest (largest) CO amplitudes occur on days with the largest (smallest) amounts of incoming shortwave radiation and the largest (smallest) diurnal temperature ranges, which

*Table 3*. CO amplitude in different seasons from other mountaintops in the literature at which CO has been studied. CO amplitudes are not available (NA) in all seasons at all sites.

| Mountaintop | Elevation (m) | Winter CO Amp. (ppb) | Spring CO Amp. (ppb) | Summer CO Amp. (ppb) | Fall CO Amp. (ppb) | Reference |
|---|---|---|---|---|---|---|
| Mount Kenya | 3678 | 9 | 15 | 25 | 20 | Henne et al., 2008 |
| Jungfraujoch | 3580 | 3 | 10 | 11 | 5 | Forrer et al., 2000 |
| Lulin Atmospheric Background Station | 2862 | 22 | 16 | 20 | 23 | Ou-Yang et al., 2014 |
| Mount Bachelor | 2763 | NA | 8 | NA | NA | Weiss-Penzais et al., 2006 |
| Mei-Feng, Taiwan | 2269 | 50 | 20 | 10 | 75 | Lin et al., 2011 |
| Whistler | 2182 | 3 | 3 | 5 | 3 | MacDonald et al., 2011 |
| Mount Tai | 1534 | NA | NA | 110 | 100 | Gao et al., 2005 |
| Pinnacles | 1017 | 7 | 5 | 4 | 6 | This study |

is in contrast to previous studies on the diurnal CO variability at other mountaintops (e.g. Gao et al., 2005).

Independent of season, the largest diurnal CO changes oftentimes occur on timescales $<3$ h and are independent of time of day. For example, CO increased from 145 ppb to 241 ppb between 0600 and 0800 LST on 11 April 2009. Synoptic analyses reveal that a cold front passed through the region during this time, inducing a wind shift from the southwest to northwest that resulted in a short-lived CO increase, during which CO mixing ratios remained $>200$ ppb for 2 h. Analysis of other variables measured on-site indicates that this CO increase was accompanied by a $CO_2$ increase and water vapour decrease. HYSPLIT backward trajectories (not shown) indicate that the prefrontal air originated over the southeastern US and had less contact with surface emissions than the post-frontal trajectories that passed over polluted regions in the northeastern US prior to arriving at Pinnacles.

Another example of a large CO change was on 26 January 2011 when CO mixing ratios increased from 176 ppb to 322 ppb between 1400 and 1600 LST during the passage of a coastal winter storm east of Pinnacles. Consistent with the 11 April 2009 frontal passage, the CO increase during the 26 January event coincided with a $CO_2$ increase and water vapour decrease. HYSPLIT trajectory analyses show that the CO, $CO_2$ and water vapour changes were caused by an air mass change that occurred as the coastal storm moved away from Pinnacles, resulting in polluted air from the northeastern US being transported to Pinnacles.

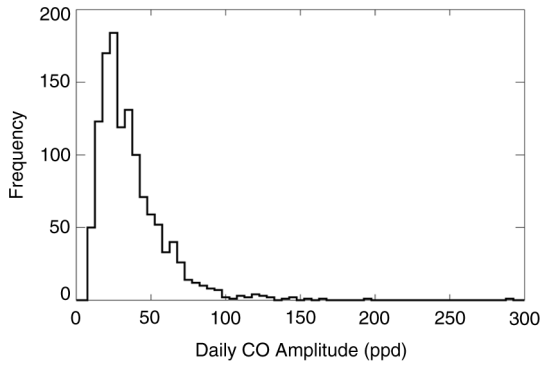


*Fig. 6*. Frequency distribution of daily CO amplitude, defined as the difference between the daily maximum and minimum half-hour CO mixing ratio, from 1 January 2009 to 31 December 2012 at 17 m agl at Pinnacles. Each bin size is 5 ppb.

From these examples, as well as from other cases not discussed, we conclude that the largest diurnal CO changes occur in the presence of synoptic disturbances, which induce wind shifts that transport air from polluted upwind source regions to Pinnacles. This finding is consistent with our hypothesis stated in Section 1, as well as with previous studies in flat terrain (e.g. Hurwitz et al., 2004) and at mountaintops (e.g. Zellwegger et al., 2003; Brooks et al., 2012) including Pinnacles (Lee et al., 2012). However, our finding that days with the smallest CO amplitude typically occur on days with strong insolation appears counter-intuitive and is contrary to our hypothesis. Strong insolation is expected to facilitate the vertical transport of air from upwind valleys to nearby mountaintops by convective mixing and upslope flows, processes which induce large changes in pollutant concentrations on diurnal timescales (e.g. Baltensperger et al., 1997; Lugauer et al., 1998). To better understand this apparent contradiction, we isolate fair weather days and investigate the CO variability on these days in the next section.

### 3.5. *CO variability on fair weather days*

We identify fair weather days by calculating a clearness index (CI) for each day in the 4-yr data set using solar radiation measurements. Following Whiteman and Allwine (1986), we calculate the maximum total incoming solar radiation that could be received at Pinnacles (i.e. the theoretical maximum). We then sum the total amount of incoming solar radiation measured at Pinnacles and divide

this value by the theoretical maximum to determine the CI (Whiteman et al., 1999a). We find that CO amplitude decreases as a function of CI. This pattern is most apparent when binning the CO amplitude into different categories based on CI. Days with the smallest CI have both the largest mean CO amplitudes and largest interquartile ranges. Furthermore, the 90th percentile of these cases have CO amplitudes $>80$ ppb, whereas the clearest days have CO amplitudes approximately half this value (Fig. 7). Days with low CI are typically cloudy, rather than hazy, based on web camera images from the site, and have stronger winds than days with high CI. Mean 17 m wind speeds on days with the lowest (highest) CI are around 5.3 m $s^{-1}$ (3.8 m $s^{-1}$) because cloudy days are more prone to the impacts of synoptic disturbances, which induce higher wind speeds, and result in larger daily changes in CO mixing ratios (c.f. Section 3.4). In contrast, days with higher CI are not impacted by synoptic disturbances, and thus the CO amplitudes on these days are usually smaller. We classify days with a high CI as fair weather days, using a CI threshold of 0.6 (i.e. above the 50th percentile). We note, though, that our results are not significantly impacted by our choice of the CI threshold.

Our analyses reveal that there are fair weather days with large diurnal CO amplitudes and with small diurnal CO amplitudes, and thus we further investigate the factors causing this variability. Since advective processes are a major factor in determining the local rate of change of a trace gas mixing ratio, we focus next on a discussion of the role of horizontal wind speed and direction on the CO variability. Previous work has found that diurnal wind direction changes are an important component of the climatology at other mountaintop monitoring sites (e.g. Atlas and Ridley, 1996; Kleissl et al., 2007). These wind direction changes are attributed to thermal circulations and are associated with the transport of pollutant-rich PBL air to nearby mountaintops (e.g. Baltensperger et al., 1997; Lugauer et al., 1998). Thus, to help understand the impact of wind direction changes on the CO variability at Pinnacles, we determine the mean CO mixing ratio as a function of wind direction. Winds from the east, southeast and south (southwest, west and northwest) happen 32% (45%) of the time and correspond with a mean CO mixing ratio of 147.5 ppb (141.8 ppb) (Fig. 8). Southerly winds have already been shown to correlate with higher CO and $CO_2$ mixing ratios during the cool season in previous studies at the site (Lee et al., 2012), which is consistent with other seasons as well. Because wind shifts to the south are an important part of the climatology at Pinnacles (c.f. Fig. 2c) and are associated with higher CO mixing ratios, we hypothesise that the CO variability on fair weather days can be explained by the presence or absence of a wind shift to the south during the daytime. Therefore, we use Pinnacles' wind measurements and classify fair weather days based on the presence or absence of a southerly wind shift. We first determine the mean wind direction for four 6-hour periods: 00–06 LST, 06–12 LST, 12–18 LST and 18–00 LST. Ninety percent of the 628 fair weather days had a CO record $>50\%$ complete during the day and are investigated further (Table 4). Forty-nine percent of these days have a steady wind direction throughout the day, i.e. the wind direction varied by $<90^{\circ}$. Consistent with the climatology discussed in Section 3.1, northwesterly winds are most common and occur predominantly during the winter months. Of the fair weather days with a constant wind direction, 67% have northwesterly winds throughout the day, whereas 4% have mean winds from the northeast. Since northwesterly winds are most common and because CO varies as a function of wind direction (Fig. 8), we classify days as Type I if the mean wind direction in each 6-h period is from the northwest.

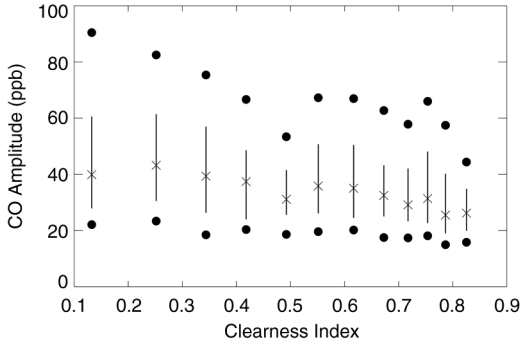


*Fig. 7.* Daily CO amplitude as a function of clearness index, divided into 12 bins ($N=78$) for each bin), from 1 January 2009 to 31 December 2012. Black X's represent 50th percentile; lines extend out to 25th and 75th percentiles; black circles represent the 10th and 90th percentiles.

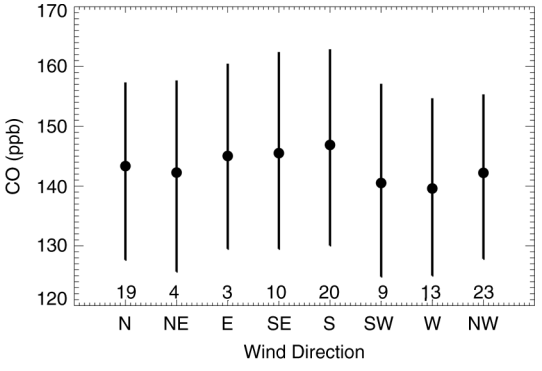


*Fig. 8.* Mean CO mixing ratio $\pm 1$ standard deviation as a function of wind direction for all days from 1 January 2009 to 31 December 2012 at 17 m agl at Pinnacles. Numbers shown are the percentage of the total. Numbers do not add to 100% because of rounding.

The remaining 51% of the fair weather days have a wind shift. A wind shift from the northwest during the first half of the day (00–12 LST) to a different wind direction during the second half of the day (12–24 LST) is most common and happens on 48% of this subset of days. On 56%, 35% and 9% of this subset of days, there is an afternoon counter clockwise wind shift to the southwest, southeast and northeast, respectively. We classify days with an afternoon wind shift to the southwest or southeast as Type II days. The remaining fair weather days have a wind shift other than what is differentiated here; they are classified as neither Type I nor Type II and are revisited in Section 3.5.3. In summary, 33 and 22% of all fair weather days are classified as Type I and Type II days, respectively.

Type I and Type II days have the similar mean CI (0.75). Mean afternoon (1200–1600 LST) shortwave radiation for Type I and Type II days is 624 W $m^{-2}$ and 633 W $m^{-2}$, respectively, whereas mean afternoon sensible heat fluxes on Type I and Type II days are 171 W $m^{-2}$ and 206 W $m^{-2}$, respectively. There are no seasonal differences in the occurrences of Type I or Type II days, although days with strong (weak) mean winds are most common in winter (summer) (Table 5) which is consistent with the climatology (c.f. Fig. 2). Synoptic analyses indicate that Type I days are most common following cold front passages, and mean winds are 0.7 m $s^{-1}$ higher than on Type II days. The diurnal behaviour of wind direction on Type I and Type II days at Pinnacles also happens at Big Meadows and nearby monitoring sites in flat terrain.

We use NARR to characterise the synoptic conditions on Type I and Type II days and to investigate the underlying causes of the wind shift on Type II days. Both Type I days and Type II days have a near-surface anticyclone southwest of Pinnacles. Consistent with Type I days, composites of the 900 mb (i.e. the approximate elevation of Pinnacles) wind fields at 0900 UTC (0400 LST) on Type II days indicate the presence of northwesterly flows across Virginia (Fig. 9a). Consistent with the observations, NARR composites of the 900 mb wind fields indicate a counter clockwise wind shift on Type II days, with southwesterly winds in the afternoon. This wind shift is most pronounced in the lee of the Appalachian Mountains, (Fig. 9b). This diurnal wind shift is also present in the surface (10 m agl) NARR composites. The mean v-component of the wind along and immediately east of the Blue Ridge Mountains is $-1$ m $s^{-1}$ (northerly) in the 0900 UTC NARR composites, but is $+2$ m $s^{-1}$ (southerly) on the 2100 UTC NARR composites (not shown). These wind shifts have been documented in previous studies in other mountainous regions, for example, the European Alps (e.g. Lugauer and Winkler, 2005) and Rocky Mountains (e.g. Whiteman et al., 1999b), and have been attributed to the diurnal cycle of diabatic heating (e.g. Whiteman, 2000). The wind shift that we observe is also present several hundred kilometres away from the Appalachian Mountains, and it is not clear if these wind shifts are caused by the diabatic heating of the mountain slopes in this region or by other processes such atmospheric tides (e.g. Mass et al., 1991).

*3.5.1. Type I days.* On Type I days, both the mean and median diurnal CO cycles exhibit a decrease between 0000 LST and 0800 LST when winds are from the northwest, consistent with the diurnal CO cycles shown in Fig. 5. Following a short-lived mid-morning CO maximum, CO decreases to a minimum between 1400 and 1800 LST and closely follows the diurnal cycle in water vapour (Fig. 10). Following the afternoon CO minimum, CO begins increasing due to pollutants accumulating within a stabilising PBL. Differentiating by mean wind speed, we find that there is a short-lived CO and water vapour maximum around 1000 LST that likely coincides with the arrival of valley PBL air at the mountaintop on days with weak winds (and thus less synoptic forcing). Following the short-lived CO increase, mixing and dilution within the growing daytime PBL result in a late afternoon CO minimum at Pinnacles.

*Table 4.* Number and percentage of fair weather days with steady winds and fair weather days without steady winds

| Classification of fair weather days | Number | Percentage of fair weather days |
|---|---|---|
| >50% data coverage | 565 | 100 |
| Steady winds | 277 | 49 |
| Steady northwesterly winds (Type I) | 187 | 33 |
| Days with a wind shift | 288 | 51 |
| Days with a wind shift from northwesterly to southerly (Type II) | 126 | 22 |
| Days that are not Type I or Type II | 252 | 45 |

*Table 5.* Occurrence of Type I and Type II days as a function of season

| | Winter | Spring | Summer | Fall |
|---|---|---|---|---|
| Type I, all | 14.2 | 15.8 | 10.9 | 10.7 |
| Type I, light winds (<3.9 m $s^{-1}$) | 4.2 | 7.6 | 9.0 | 4.9 |
| Type I, strong winds (>3.9 m $s^{-1}$) | 9.7 | 8.2 | 1.9 | 5.8 |
| Type II, all | 9.2 | 11.4 | 8.4 | 9.1 |
| Type II, light winds (<3.3 m $s^{-1}$) | 1.7 | 3.3 | 6.5 | 5.5 |
| Type II, strong winds (>3.3 m $s^{-1}$) | 7.5 | 7.1 | 3.0 | 2.7 |

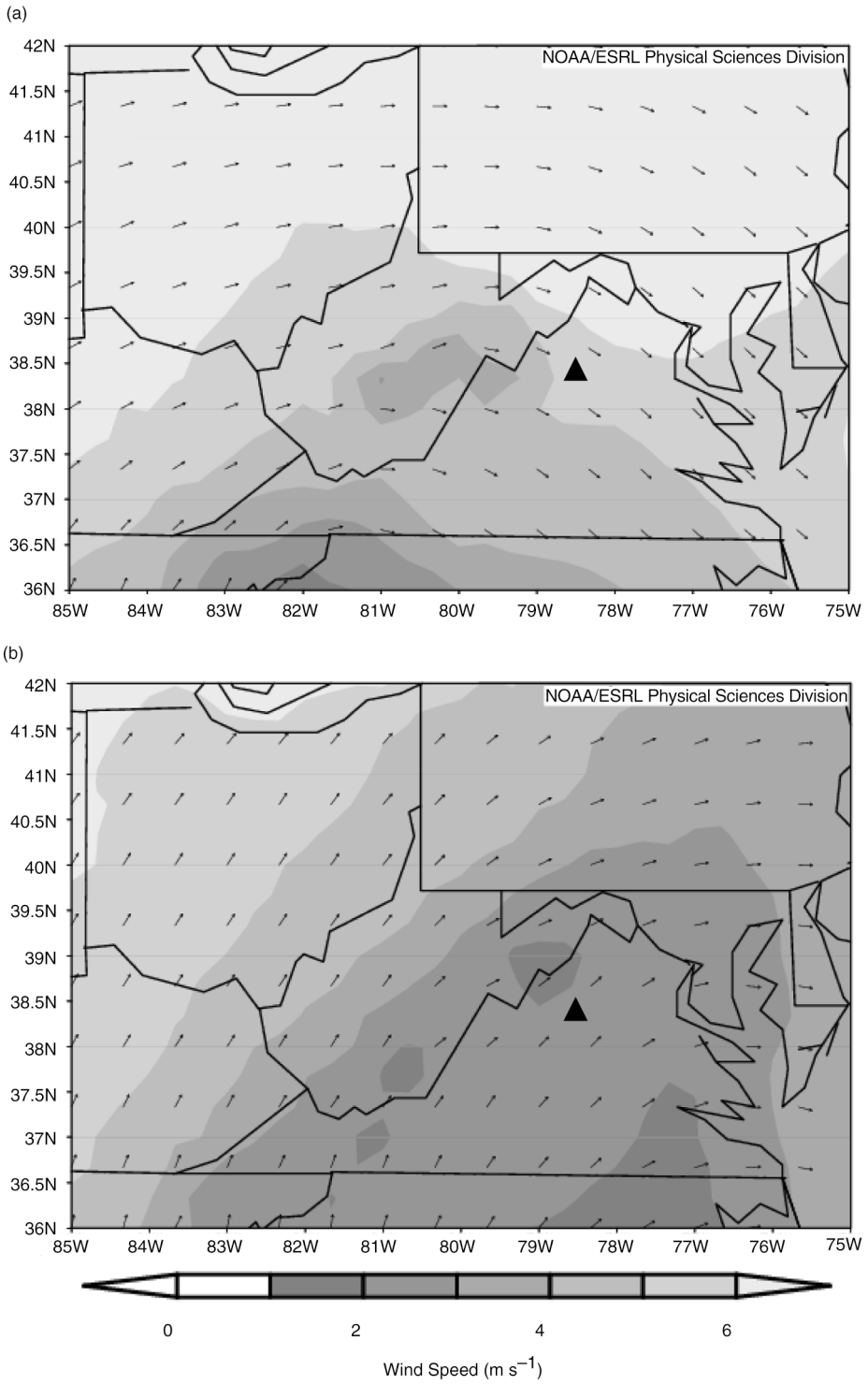


*Fig. 9.* NARR composites on Type II days of 900 mb wind speed and direction at 0900 UTC (a) and 2100 UTC (b). The location of Pinnacles is indicated by a black triangle. Data are available from <ftp://ftp.cdc.noaa.gov/NARR/>

The observed CO variability on Type I days contrasts with findings on the diurnal trace gas and aerosol variability at other mountaintops at which the vertical transport of valley PBL air causes a daytime trace gas and aerosol increase (e.g. Baltensperger et al., 1997; Weiss-Penzias et al., 2006) and also contrasts with the mean seasonal diurnal

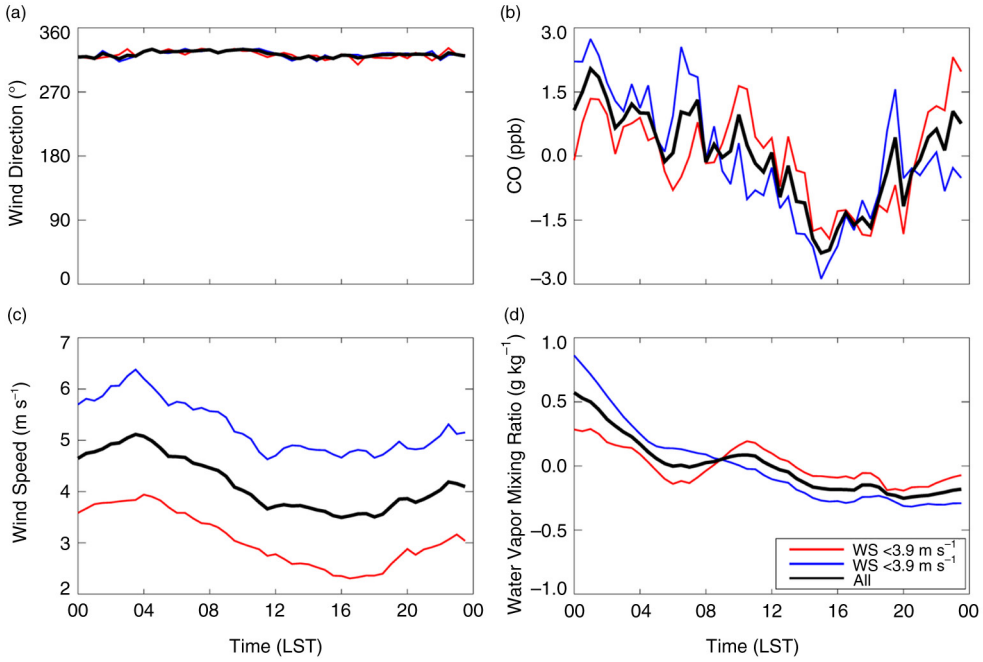


*Fig. 10.* Mean wind direction (a), CO (b), wind speed (c) and water vapour (d) on Type I fair weather days. Red, blue and black lines represent Type I days with light winds ( $<3.9\,\mathrm{m\,s^{-1}}$, $N=94$), Type I days with strong winds ( $>3.9\,\mathrm{m\,s^{-1}}$, $N=93$), and all Type I days ($N=187$), respectively. Daily means are removed from panels (b) and (d) for clarity. All measurements are made at 17 m agl at Pinnacles.

cycles of CO at Pinnacles. The presence of constant wind directions throughout the entire diurnal cycle at Pinnacles is an important characteristic of the diurnal CO variability on Type I days with a daytime CO minimum. This diurnal cycle has been reported for other trace gas species. For example, peroxyacetic nitric anhydride (PAN), which depending on ambient temperature has a relatively long atmospheric lifetime (e.g. Seinfeld and Pandis, 1996) that enables it to be transported over long distances (e.g. Fahey et al., 1986), was sampled at a mountaintop monitoring site approximately 360 km southwest of Pinnacles in the late 1980s (e.g. Roberts et al., 1995). Consistent with our findings in the diurnal CO cycle on Type I days, the mean diurnal cycle in PAN during the summertime shows a daytime decrease (Roberts et al., 1995). This daytime decrease is consistent with the diurnal cycle of trace gas variability over flat terrain (e.g. Popa et al., 2010). A few hundred metres above the surface in flat terrain, there is oftentimes a short-lived mid-morning trace gas increase due to the arrival of polluted air contained within the nocturnal PBL (e.g. Schmidt et al., 2014). As the PBL increases in depth, turbulent mixing within the PBL causes trace gas mixing ratios to decrease (e.g. Popa et al., 2010; Schmidt et al., 2014). The PBL depth represents the height to which turbulent mixing dominates and is an important driver of trace gas and aerosol variability over flat terrain (e.g. Seibert et al., 2000; Gibert et al., 2007) and in valleys (e.g. Pal et al., 2014).

Based on the findings in the present study, the PBL height is similarly expected to be another important driver of the CO variability at mountaintops like Pinnacles, in particular on Type I days. Continuous PBL height observation platforms for Pinnacles and its immediate surroundings are not available for the entire study period. The sounding station nearest Pinnacles where twice-daily rawinsonde observations are available is Dulles Airport (IAD), which is located 90 km northeast of Pinnacles. If we assume that PBL heights from the IAD rawinsonde observations are the same as at Pinnacles, we find that days with deep PBLs (i.e. those exceeding the mountaintop height) have a daytime CO decrease, consistent with what we find for Type I days. In a forthcoming paper we investigate in more detail how PBL heights near Pinnacles affect the mountaintop trace gas variability.

*3.5.2. Type II days.* On Type II days, an afternoon shift in wind direction has a significant effect on CO variability, and the amplitude of both the median and mean CO cycle is about twice the amplitude of Type I days (Fig. 11), illustrating the dominance of horizontal advection over vertical mixing. During the night-time, CO decreases. As winds begin to shift towards the south during the late morning, CO and water vapour begin increasing and peak around 1900 LST. Strong mechanical mixing causes smaller CO peaks on days with strong winds compared to days

with weak winds. Following the daytime increase, CO decreases as winds shift towards the west.

Unlike Type I days, the observed pattern of CO variability on Type II days is more consistent with the mean diurnal CO cycles shown in Fig. 5 and with the mean diurnal CO cycles reported at other mountaintops (e.g. Weiss-Penzias et al., 2006; Henne et al., 2008; Obrist et al., 2008). Lee et al. (2012) found that high CO and $CO_2$ on days with south and southeast winds is caused by the near-surface transport of air masses southward from the Northeast and Mid-Atlantic and then northwestward to Pinnacles. Thus, the transport of emissions from these areas may be explain the high CO mixing ratios observed at Pinnacles during the afternoon on Type II days. However, Skyline Drive, a tourist road through SNP, is also directly upwind of Pinnacles during the afternoon on Type II days. To investigate the possible effect of Skyline Drive on the CO measurements, we select Type II days with weak winds, i.e. when Skyline Drive is expected to have the largest impact on the CO measurements, and differentiate among the seasons due to seasonal differences in traffic volume. Although emissions are typically higher during the summer and fall because of larger traffic volumes, we find no evidence of a larger afternoon peak in these seasons compared with other seasons. Furthermore, the CO maximum occurs several hours after the peak in traffic along Skyline Drive. Thus, we infer that there is no significant influence of Skyline Drive on CO mixing ratios measured at Pinnacles, which is consistent with previous studies in the region which also found no significant relation between traffic volume and $CO_2$ at Pinnacles (Lee et al., 2012), or CO (e.g. Poulida et al., 1991) and $O_3$ (e.g. Cooper and Moody, 2000) at Big Meadows.

*3.5.3. CO variability on other fair weather days.* Analysis of fair weather days not classified as Type I or Type II underscores the importance of wind shifts to the Pinnacles CO variability. On the days not classified as Type I or Type II (45% of the remaining fair weather days), the wind direction change differed from the Type II classification. Fair weather days with wind shifts to the northwest have CO decreases because, as previously discussed, northwest winds are associated with lower CO mixing ratios than southerly winds. Conversely, fair weather days with southerly wind shifts have daytime CO increases. These characteristics of the CO variability on days not classified as Type I or Type II highlight the finding that, when wind direction changes occur at Pinnacles, they have a greater impact on the diurnal CO variability than PBL dilution.

## 4. Conclusions and implications

In this study, we presented an overview of 4 yr (1 January 2009–31 December 2012) of meteorological and CO

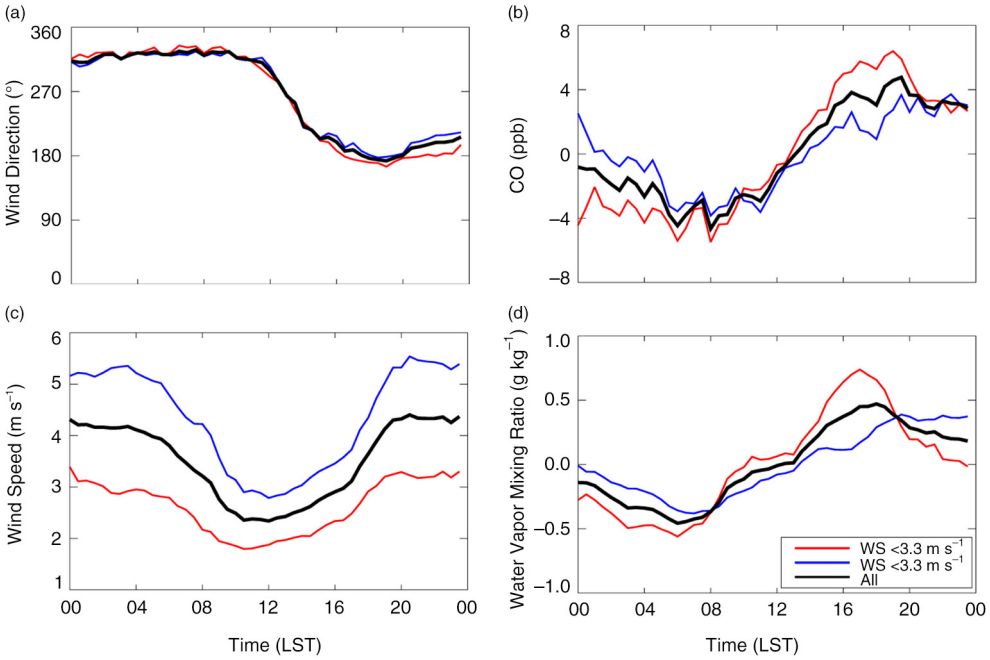


*Fig. 11.* Same as Fig. 10 but for Type II days. Red, blue and black lines represent Type II days with light winds ( $<3.3\,m\,s^{-1}$, $N=62$), Type II days with strong winds ( $>3.3\,m\,s^{-1}$, $N=64$) and all Type II days ($N=126$), respectively. Note the y-axes in panels (b) and (c) are different from Fig. 10.

measurements from Pinnacles, a new mountaintop monitoring site in the Appalachian Mountains, and investigated the hypothesis that the largest CO variability occurs during cold front passages and on fair weather days due to the transport of polluted PBL air to the mountaintop. We found that CO typically increases from a minimum between 0500 and 0900 LST to a maximum between 1600 and 2000 LST. Consistent with our hypothesis, the largest CO changes, with half-hourly means up to 320 ppb, occur in the presence of synoptic disturbances, as previously found for $CO_2$ changes at the site (Lee et al., 2012). Contrary to our hypothesis, though, the smallest CO changes happen on fair weather days (i.e. days with a CI $> 0.6$ and about 50% of all days), which we further investigated by classifying fair weather days into two regimes based on the presence or absence of a wind shift. On days with steady northwesterly winds at the site (Type I days or 33% of the fair weather days), mixing and dilution within the daytime PBL is the dominant driver of CO variability. Thus, daytime PBL heights are an important driver of the trace gas variability at the site and are investigated in detail in a forthcoming study.

On days with a wind shift from the northwest to the south (Type II days or 22% of the fair weather days), the CO increase is about twice the magnitude of the CO change on days without wind shifts, and the site samples different upwind source regions. From these analyses, we conclude that the diurnal CO cycle at Pinnacles is largely driven by a daytime wind shift to the south which causes a daytime CO increase. This wind shift happens not only on Type II days, but is an important part of the climatology (Fig. 2c) and is partly driven by synoptic-scale forcings (i.e. frontal passages) and by local- to mesoscale forcings (i.e. diurnal mountain circulations).

The results in this study provide new insights into the use of trace gas measurements from low mountaintops like Pinnacles in applications that require background trace gas measurements. The nighttime CO decrease and daily minimum between 0500 and 0900 LST present in the mean diurnal CO cycle indicate the transport of FA air to the site. Therefore, pre-dawn trace gas measurements, particularly those in winter, are likely to be most representative of background CO values.

When we differentiated between fair weather days with a wind shift and days without a wind shift, we found that the diurnal CO variability is analogous to findings from other, taller mountaintops (e.g. Forrer et al., 2000; Balzani Lööv et al., 2008; Henne et al., 2008; Obrist et al., 2008) on fair weather days with a wind shift. The wind shift results in different upwind emission sources being sampled and may allow trace gas measurements from Pinnacles to help estimate emissions and reduce uncertainties in flux estimates (e.g. Schuh et al., 2010), provided that the models accurately represent atmospheric transport over complex terrain.

Finally, our findings are the first to indicate that, in other conditions (i.e. fair weather days with steady winds), CO mixing ratios at low mountaintops like Pinnacles decrease during the daytime, which is nearly identical to what happens at tall towers in flat terrain. As noted earlier, there is a short-lived late morning CO increase that occurs both atop tall towers and at Pinnacles. Whereas the increase atop tall towers is caused by the arrival of polluted nocturnal PBL air (e.g. Yi et al., 2001; Pal et al., 2015), the increase at mountaintops is caused by the arrival of polluted PBL air contained within the nocturnal valley PBL. As the PBL depth increases, CO decreases at the tops of tall towers and at low mountaintops like Pinnacles. Thus, local impacts on afternoon trace gas measurements made during these situations (i.e. about 60% of the days without clouds) are expected to be minimised, and mountaintop trace gas measurements can be considered along with tall tower measurements in applications requiring regionally representative values.

## 5. Acknowledgements

This research and maintenance of the Pinnacles research station was partly funded by an MOU between the NOAA ESRL Global Monitoring Division and the University of Virginia and by NSF-CAREER Grant ATM-1151445. The authors thank staff from SNP, especially Elizabeth Garcia and Alan Williams, and students from the Environmental Sciences Department at the University of Virginia for helping to maintain data collection at Pinnacles, especially Nevio Babić, Stephanie Phelps and Mark Sghiatti. Many thanks to Zeljko Vecenaj at the University of Zagreb for on-site support in 2008, 2009 and 2012, and to Jonathan Williams at NOAA ESRL. We also thank the anonymous reviewer whose suggestions helped us improve the manuscript.

## References

Andrews, A. E., Kofler, J. D., Trudeau, M. E., Williams, J. C., Neff, D. H. and co-authors. 2014. $CO_2$, CO, and $CH_4$ measurements from tall towers in the NOAA Earth System Research Laboratory's Global Greenhouse Gas Reference Network: instrumentation, uncertainty analysis, and recommendations for future high-accuracy greenhouse gas monitoring efforts. *Atmos. Meas. Tech.* **7**, 647–687. DOI: 10.5194/amt-7-647-2014.

Atlas, E. L. and Ridley, B. A. 1996. The Mauna Loa observatory photochemistry experiment: introduction. *J. Geophys. Res.* **101**(D9), 14531–14541.

Bakwin, P. S. and Tans, P. P. 1995. Measurements of carbon dioxide on a very tall tower. *Tellus B.* **47**, 535–549. DOI: 10.1034/j.1600-0889.47.issue5.2.x.

Baltensperger, U., Gäggeler, H. W., Jost, D. T., Lugauer, M., Schwikowski, M. and co-authors. 1997. Aerosol climatology at the high-alpine site Jungfraujoch, Switzerland. *J. Geophys. Res.* **102**(D16), 19707–19715. DOI: 10.1029/97JD00928.

Balzani Lööv, J. M., Henne, S., Legreid, G., Staehelin, J., Reimann, S. and co-authors. 2008. Estimation of background concentrations of trace gases at the Swiss alpine site Jungfraujoch (3580 m asl). *J. Geophys. Res.* **113**(D22305). DOI: 10.1029/2007JD009751.

Brooks, B. G. J., Desai, A. R., Stephens, B. B., Bowling, D. R., Burns, S. P. and co-authors. 2012. Assessing filtering of mountaintop $CO_2$ mole fractions for application to inverse models of biosphere-atmosphere carbon exchange. *Atmos. Chem. Phys.* **12**, 2099–2115. DOI: 10.5194/acp-12-2099-2012.

Cooper, O. R. and Moody, J. L. 2000. Meteorological controls on ozone at an elevated eastern United States regional background monitoring site. *J. Geophys. Res.* **105**(D5), 6855–6869. DOI: 10.1029/1999JD901015.

Crutzen, P. J. and Andreae, M. O. 1990. Biomass burning in the tropics: impact on atmospheric chemistry and biogeochemical cycles. *Science*. **250**(4988), 1669–1678. DOI: 10.1126/science.250.4988.1669.

De Wekker, S. F. J., Ameen, A., Song, G., Stephens, B. B., Hallar, A. G. and co-authors. 2009. A preliminary investigation of boundary layer effects on daytime atmospheric $CO_2$ concentrations at a mountaintop location in the Rocky Mountains. *Acta. Geophys.* **57**, 904–922. DOI: 10.2478/s11600-009-0033-6.

De Wekker, S. F. J., Steyn, D. G. and Nyeki, S. 2004. A comparison of aerosol-layer and convective boundary-layer structure over a mountain range during STAARTE '97. *Boundary Layer Meteorol.* **113**(2), 249–271. DOI: 10.1023/B:BOUN.0000039371.41823.37.

Draxler, R. R. and Hess, G. D. 2004. *Description of the HYSPLIT 4 Modeling System (NOAA Technical Memorandum ERL ARL-224)*. NOAA Air Resources Laboratory, Silver Spring, MD.

Fahey, D. W., Hübler, G., Parrish, D. D., Williams, E. J., Norton, R. B. and co-authors. 1986. Reactive nitrogen species in the troposphere: measurements of NO, $NO_2$, $HNO_3$, Particulate Nitrate, Peroxyacetyl Nitrate (PAN), $O_3$, and total reactive odd nitrogen ($NO_y$) at Niwot Ridge, Colorado. *J. Geophys. Res.* **91**(D9), 9781–9783. DOI: 10.1029/JD091iD09p09781.

Forrer, J., Rüttimann, R., Schneiter, D., Fischer, A., Buchmann, B. and co-authors. 2000. Variability of trace gases at the high-Alpine site Jungfraujoch caused by meteorological transport processes. *J. Geophys. Res.* **105**(D10), 12241–12251. DOI: 10.1029/1999JD901178.

Gao, J., Wang, T., Ding, A. and Liu, C. 2005. Observational study of ozone and carbon monoxide at the summit of mount Tai (1534 m a.s.l.) in central-eastern China. *Atmos. Environ.* **39**, 4779–4991. DOI: 10.1016/j.atmosenv.2005.04.030.

Gerbig, C., Dolman, A. J. and Heimann, M. 2009. On observational and modelling strategies targeted at regional carbon exchange over continents. *Biogeosciences*. **6**, 1949–1959.

Gibert, F., Schmidt, M., Cuesta, J., Ciais, P., Ramonet, M. and co-authors. 2007. Retrieval of average $CO_2$ fluxes by combining in situ $CO_2$ measurements and backscatter lidar information. *J. Geophys. Res.* **112**(D10301). DOI: 10.1029/2006JD008190.

Giglio, L., Descloitres, J., Justice, C. O. and Kaufman, Y. J. 2003. An enhanced contextual fire detection algorithm for MODIS. *Remote. Sens. Environ.* **87**, 273–282. DOI: 10.1016/S0034-4257(03)00184-6.

Gloor, M., Bakwin, P., Hurst, D., Lock, L., Draxler, R. and co-authors. 2001. What is the concentration footprint of a tall tower? *J. Geophys. Res.* **106**, 17831–17840. DOI: 10.1029/2001JD900021.

Greco, S. and Baldocchi, D. D. 1996. Seasonal variations of $CO_2$ and water vapour exchange rates over a temperate deciduous forest. *Global Change Biol.* **2**, 183–197. DOI: 10.1111/j.1365-2486.1996.tb00071.x.

Henne, S., Dommen, J., Neininger, B., Reimann, S., Staehelin, S. and co-authors. 2005. Influence of mountain venting in the Alps on the ozone chemistry of the lower free troposphere and the European pollution export. *J. Geophys. Res.* **110**(D22307). DOI: 10.1029/2005JD005936.

Henne, S., Furger, M., Nyeki, S., Steinbacher, M., Neininger, B. and co-authors, 2004. Quantification of topographic venting of boundary layer air to the free troposphere. *Atmos. Chem. Phys.* **4**, 497–509.

Henne, S., Klausen, J., Junkermann, W., Kariuki, J. M., Aseyo, J. O. and co-authors, 2008. Representativeness and climatology of carbon monoxide and ozone at the global GAW station Mt. Kenya in equatorial Africa. *Atmos. Chem. Phys.* **8**, 3119–3139.

Hurwitz, M. D., Ricciuto, D. M., Bakwin, P. S., Davis, K. J., Wang, W. and co-authors. 2004. Transport of carbon dioxide in the presence of storm systems over a northern Wisconsin forest. *J. Atmos. Sci.* **61**, 607–618. DOI: 10.1175/15200469(2004)061 < 0607:TOCDIT > 2.0.CO;2.

Igarashi, Y., Sawa, Y., Yoshioka, K., Takahashi, H., Matsueda, H. and co-authors. 2006. Seasonal variations in SO2 plume transport over Japan: observations at the summit of Mt. Fuji from winter to summer. *Atmos. Environ.* **40**, 7018–7033. DOI: 10.1016/j.atmosenv.2006.06.017.

Jaffe, D., Prestbo, E., Swartzendruber, P., Weiss-Penzias, P., Kato, S. and co-authors. 2005. Export of atmospheric mercury from Asia. *Atmos. Environ.* **39**, 3029–3038. DOI: 10.1016/j.atmosenv.2005.01.030.

Janjic, Z., Black, T., Pyle, M., Ferrier, B., Chuang, H. Y. and co-authors. 2011. *User's Guide for the NMM Core of the Weather Research and Forecast (WRF) Modeling System Version 3*. National Center for Atmospheric Research, Boulder, CO, pp. 95.

Janjic, Z., Gall, R. and Pyle, M. E. 2010. *Scientific Documentation for the NMM Solver*. NCAR Tech. Note NCR/TN 477 + STR. pp. 54.

Justice, C. O., Giglio, L., Korontzi, S., Owens, J., Morisette, J. and co-authors. 2002. The MODIS fire products. *Rem. Sens. Environ.* **83**, 244–262. DOI: 10.1016/S0034-4257(02)00076-7.

Kleissl, J., Honrath, R. E., Dziobak, M. P., Tanner, D., Val Martín, M. and co-authors. 2007. Occurrence of upslope flows at the Pico mountaintop observatory: a case study of orographic flows on a small, volcanic island. *J. Geophys. Res.* **112**(D10S35). DOI: 10.1029/2006JD007565.

Lac, C., Donnelly, R. P., Masson, V., Pal, S., Riette, S. and co-authors. 2013. $CO_2$ dispersion modelling over Paris region within the $CO_2$-MEGAPARIS project. *Atmos. Chem. Phys.* **13**, 4941–4961.

Lee, T. R. 2015. The impact of planetary boundary layer dynamics on mountaintop trace gas variability. Ph.D. Dissertation, University of Virginia, pp. 213.

Lee, T. R., De Wekker, S. F. J., Andrews, A. E., Kofler, J. and Williams, J. 2012. Carbon dioxide variability during cold front passages and fair weather days at a forested mountaintop site. *Atmos. Environ.* **46**, 405–416. DOI: 10.1016/j.atmosenv.2011.09.068.

Lee, T. R., De Wekker, S. F. J. and Wofford, J. E. B. 2014. Downscaling maximum temperature projections to subkilometer resolutions in the Shenandoah National Park of Virginia, USA. *Adv. Meteorol.* **2014**. DOI: 10.1155/2014/594965.

Levin, I., Graul, R. and Trivett, N. B. A. 1995. Long-term observations of atmospheric $CO_2$ and carbon isotopes at continental sites in Germany. *Tellus B.* **47**, 23–34. DOI: 10.1034/j.1600-0889.47.issue1.4.x.

Lin, Y. C., Lin, C. Y., Lin, P. H., Engling, G., Lan, Y.-Y. and co-authors. 2011. Observations of ozone and carbon monoxide at Mei-Feng mountain site (2269 m a.s.l.) in Central Taiwan: seasonal variations and influence of Asian continental outflow. *Sci. Total Environ.* **409**, 3033–3042. DOI: 10.1016/j.scitotenv.2011.04.023.

Lugauer, M., Baltensperger, U., Furger, M., Gäggeler, H. W., Jost, D. T. and co-authors. 1998. Aerosol transport to the high Alpine sites Jungfraujoch (3454 m asl) and Colle Gnifetti (4452 m asl). *Tellus.* **50**, 76–92. DOI: 10.1034/j.1600-0889.1998.00006.x.

Lugauer, M. and Winkler, P. 2005. Thermal circulation in South Bavaria – climatology and synoptic aspects. *Meteorol. Z.* **14**, 15–30. DOI: 10.1127/0941-2948/2005/0014-0015.

MacDonald, A. M., Anlauf, K. G., Leaitch, W. R., Chan, E. and Tarasick, D. W. 2011. Interannual variability of ozone and carbon monoxide at the Whistler high elevation site: 2002–2006. *Atmos. Chem. Phys.* **11**, 11431–11446. DOI: 10.5194/acp-11-11431-2011.

Mass, C. F., Steenburgh, W. J. and Schultz, D. M. 1991. Diurnal surface-pressure variations over the continental United States and the influence of sea level reduction. *Mon. Weather Rev.* **119**, 2814–2830. DOI: 10.1175/1520-0493(1991)119<2814:DSPVOT>2.0.CO;2.

Mesinger, F., DiMego, G., Kalnay, E., Mitchell, K., Shafran, P. C. and co-authors. 2006. North American regional reanalysis. *Bull. Am. Meteorol. Soc.* **87**, 343–360. DOI: 10.1175/BAMS-87-3-343.

Necki, J., Schmidt, M., Rozanski, K., Zimnoch, M., Korus, A. and co-authors. 2003. Six-year record of atmospheric carbon dioxide and methane at a high-altitude mountain site in Poland. *Tellus B.* **55**, 94–104k. DOI: 10.1034/j.1600-0889.2003.01446.x.

Novelli, P. C., Masarie, K. A. and Lang, P. M. 1998. Distributions and recent changes of carbon monoxide in the lower troposphere. *J. Geophys. Res.* **103**(D15), 19015–19033. DOI: 10.1029/98JD01366.

Obrist, D., Hallar, A. G., McCubbin, I., Stephens, B. B. and Rahn, T. 2008. Atmospheric mercury concentrations at Storm Peak Laboratory in the Rocky Mountains: evidence for long-range transport from Asia, boundary layer contributions, and plant mercury uptake. *Atmos. Environ.* **42**, 7579–7589. DOI: 10.1016/j.atmosenv.2008.06.051.

Ou-Yang, C. F., Lin, N. H., Lin, C. C., Wang, S.-H., Sheu, G. R. and co-authors. 2014. Characteristics of atmospheric carbon monoxide at a high-mountain background station in East Asia. *Atmos. Environ.* **89**, 613–622. DOI: 10.1016/j.atmosenv.2014.02.060.

Pal, S., Lee, T. R., Phelps, S. and De Wekker, S. F. J. 2014. Impact of atmospheric boundary layer depth variability and wind reversal on the diurnal variability of aerosol concentration at a valley site. *Sci. Total Environ.* **496**, 424–434. DOI: 10.1016/j.scitotenv.2014.07.067.

Pal, S., Lopez, M., Schmidt, M., Ramonet, M., Gibert, F. and co-authors. 2015. Investigation of the atmospheric boundary layer depth variability and its impact on the $^{222}$Rn concentration at a rural site in France. *J. Geophys. Res. Atmos.* **120**, 623–643. DOI: 10.1002/2014JD022322.

Pandey Deolal, S., Henne, S., Ries, L., Gilge, S., Weers, U. and co-authors. 2014. Analysis of elevated springtime levels of peroxyacetyl nitrate (PAN) at the high alpine research sites Jungfraujoch and Zugspitze. *Atmos. Chem. Phys.* **14**, 12553–12571. DOI: 10.5194/acp-14-12553-2014.

Peters, W., Jacobson, A. R., Sweeney, C., Andrews, A. E., Conway, T. J. and co-authors. 2007. An atmospheric perspective on North American carbon dioxide exchange: CarbonTracker. *Proc. Natl. Acad. Sci.* **104**(48), 18925–18930. DOI: 10.1073/pnas.0708986104.

Pillai, D., Gerbig, C., Ahmadov, R., Rödenbeck, C., Kretschmer, R. and co-authors. 2011. High-resolution simulations of atmospheric $CO_2$ over complex terrain – representing the Ochsenkopf mountain tall tower. *Atmos. Chem. Phys.* **11**, 7445–7464. DOI: 10.5194/acp-11-7445-2011.

Popa, M. E., Gloor, M., Manning, A. C., Jordan, A., Schultz, U. and co-authors. 2010. Measurements of greenhouse gases and related tracers at Bialystok tall tower station in Poland. *Atmos. Meas. Tech.* **3**, 407–427. DOI: 10.5194/amt-3-407-2010.

Poulida, O., Dickerson, R. R., Doddridge, B. G., Holland, J. Z., Wardell, R. G. and co-authors. 1991. Trace gas concentrations and meteorology in rural Virginia 1. Ozone and carbon monoxide. *J. Geophys. Res.* **96**(D12), 22461–22475. DOI: 10.1029/91JD02353.

Ramonet, M., Ciais, P., Aalto, T., Aulagnier, C., Chevallier, F. and co-authors. 2010. A recent build-up of atmospheric $CO_2$ over Europe. Part 1: observed signals and possible explanations. *Tellus B.* **62**, 1–13. DOI: 10.1111/j.1600-0889.2009.00442.x.

Roberts, J. M., Tanner, R. L., Newman, L., Bowersox, V. C., Bottenheim, J. W. and co-authors. 1995. Relationships between PAN and ozone at sites in eastern North America. *J. Geophys. Res.* **100**(22), 821–22, 830. DOI: 10.1029/95JD01221.

Schmidt, M., Graul, R., Sartorius, H. and Levin, I. 1996. Carbon dioxide and methane in continental Europe: a climatology, and $^{222}$Radon-based emission estimates. *Tellus B.* **48**, 457–473. DOI: 10.1034/j.1600-0889.1994.t01-2-00002.x-i1.

Schmidt, M., Graul, R., Satorius, H. and Levin, I. 2003. The Schauinsland $CO_2$ record: 30 years of continental observations

and their implications for the variability of the European $CO_2$ budget. *J. Geophys. Res.* **108**(D19), 4619. DOI: 10.1029/2002JD003085.

Schmidt, M., Lopez, M., Kwok, C. Y., Messager, C., Ramonet, M. and co-authors. 2014. High-precision quasi-continuous atmospheric greenhouse gas measurements at Trainou tower (Orléans forest, France). *Atmos. Meas. Tech.* **7**, 2283–2296. DOI: 10.5194/amt-7-2283-2014.

Schuh, A. E., Denning, A. S., Corbin, K. D., Baker, I. T., Uliasz, M. and co-authors. 2010. A regional high-resolution carbon flux inversion of North America for 2004. *Biogeosciences.* **7**, 1625–1644. DOI: 10.5194/bg-7-1625-2010.

Seibert, P., Beyrich, F., Gryning, S.-E., Joffre, S., Rasmussen, A. and co-authors. 2000. Intercomparison of operational methods for the determination of the mixing height. *Atmos. Environ.* **34**, 1001–1027. DOI: 10.1016/S1352-2310(99)00349-0.

Seinfeld, J. H. and Pandis, S. N. 2006. *Atmospheric Chemistry and Physics: From Air Pollution to Climate Change*. Wiley, New York, NY.

Steyn, D. G., De Wekker, S. F. J., Kossmann, M. and Martilli, A. 2012. Boundary layers and air quality in mountainous terrain. In: *Mountain Weather Research and Forecasting: Recent Progress and Current Challenges* (eds. F. K. Chow, S. F. J. De Wekker and B. J. Snyder). Springer, Dordrecht, pp. 261–289.

Thompson, A. M. 1992. The oxidizing capacity of the earth's atmosphere: probable past and future changes. *Science*. **256** (5060), 1157–1165. DOI: 10.1126/science.256.5060.1157.

Thompson, R. L., Manning, A. C., Gloor, E., Schultz, U., Seifert, T. and co-authors. 2009. In-situ measurements of oxygen, carbon monoxide and greenhouse gases from Ochsenkopf tall tower in Germany. *Atmos. Meas. Tech.* **2**, 573–591. DOI: 10.5194/amtd-2-1247-2009.

Thoning, K. W., Tans, P. P. and Komhyr, W. D. 1989. Atmospheric carbon dioxide at Mauna Loa Observatory. 2: analysis of the NOAA/GMCC data, 1974–1985. *J. Geophys. Res.* **94**(D6), 8549–8565. DOI: 10.1029/JD094iD06p08549.

Weiss-Penzias, P., Jaffe, D. A., Swartzendruber, P., Dennison, J. B., Chand, D. and co-authors. 2006. Observations of Asian air pollution in the free troposphere at Mount Bachelor Observatory during the spring of 2004. *J. Geophys. Res.* **111**, D10304. DOI: 10.1029/2005JD006522.

Whiteman, C. D. 2000. *Mountain Meteorology: Fundamentals and Applications*. Oxford University Press, Oxford, UK, p. 355.

Whiteman, C. D. and Allwine, K. J. 1986. Extraterrestrial solar radiation on inclined surfaces. *Environ. Software*. **1**(3), 164–169. DOI: 10.1016/0266-9838(86)90020-1.

Whiteman, C. D., Bian, X. and Sutherland, J. L. 1999b. Wintertime surface wind patterns in the Colorado River Valley. *J. Appl. Meteorol.* **38**, 1118–1130. DOI: 10.1175/1520-0450(1999)038 <1118:WSWPIT >2.0.CO;2.

Whiteman, C. D., Bian, X. and Zhong, S. 1999a. Wintertime evolution of the temperature inversion in the Colorado Plateau Basin. *J. Appl. Meteorol.* **38**, 1103–1117. DOI: 10.1175/1520-0450(1999)038 <1103:WEOTTI >2.0.CO;2.

Yi, C., Davis, K. J., Berger, B. W. and Bakwin, P. S. 2001. Long-term observations of the dynamics of the continental planetary boundary layer. *J. Atmos. Sci.* **58**, 1288–1299. DOI: 10.1175/1520-0469(2001)058 <1288:LTOOTD >2.0.CO;2.

Zellwegger, C., Forrer, J., Hofer, P., Nyeki, S., Schwarzenbach, B. and co-authors. 2003. Partitioning of reactive nitrogen ($NO_y$) and dependence on meteorological conditions in the lower free troposphere. *Atmos. Chem. Phys.* **3**, 779–796. DOI: 10.5194/acp-3-779-2003.

Zhao, C. L. and Tans, P. P. 2006. Estimating uncertainty of the WMO mole fraction scale for carbon dioxide in air. *J. Geophys. Res.* **111**, D08S09. DOI: 10.1029/2005JD006003.

Zimmerman, P. R., Chatfield, R. B., Fishman, J., Crutzen, P. J. and Hanst, P. L. 1978. Estimates on the production of CO and $H_2$ from the oxidation of hydrocarbon emissions from vegetation. *Geophys. Res. Lett.* **5**(8), 679–682. DOI: 10.1029/GL005i008p00679.